Structural and physical properties of $BiFeO_3$ thin films epitaxially grown on $SrTiO_3$ (001) and polar (111) surfaces*

He Shu-Min(贺树敏), Liu Guo-Lei(刘国磊)†, Zhu Da-Peng(朱大鹏), Kang Shi-Shou(康仕寿), Chen Yan-Xue(陈延学), Yan Shi-Shen(颜世申), and Mei Liang-Mo(梅良模)

School of Physics & State key Laboratory of Crystal Materials, Shandong University, Jinan 250100, *China*

(Received 3 May 2013; revised manuscript received 30 August 2013; published online 12 February 2014)

The influence of surface polarity on the structural properties of $BiFeO_3$ (BFO) thin films is investigated. BFO thin films are epitaxially grown on $SrTiO_3$ (STO) (100) and polar (111) surfaces by oxygen plasma-assisted molecular beam epitaxy. It is shown that the crystal structure, surface morphology, and defect states of BFO films grown on STO substrates with nonpolar (001) or polar (111) surfaces perform very differently. BFO/STO (001) is a fully strained tetragonal phase with orientation relationship (001)[100]BFO‖(001)[100]STO, while BFO/STO (111) is a rhombohedral phase. BFO/STO (111) has rougher surface morphology and less defect states, which results in reduced leakage current and lower dielectric loss. Moreover, BFO films on both STO (001) and STO (111) are direct band oxides with similar band gaps of 2.65 eV and 2.67 eV, respectively.

Keywords: multiferroics, $BiFeO_3$, polar surface, epitaxial growth

PACS: 68.47.Gh, 77.55.Nv, 77.55.Px **DOI:** 10.1088/1674-1056/23/3/036801

1. Introduction

$BiFeO_3$ (BFO) has attracted great attention due to its room-temperature multiferroic properties and potential applications in spintronic devices.[1–4] Since BFO has high remanent polarization, it has been considered as one of the lead-free candidates for high-density ferroelectric random access memories (FeRAMs).[4] Below Curie temperature T_C = 1100 K, bulk BFO is a rhombohedrally distorted perovskite with a stretch along one of the four [111] crystallographic directions.[5,6] When grown as thin films, rich structural and physical properties arise from the interplay between electronic and lattice degrees of freedom tuned by epitaxial strain.[7–9] The ferroelectric polarization, coercive field, and leakage current of BFO thin films, can be modified via coupling between corresponding order parameters and lattice.[7,9] A great deal of experimental effort has been devoted to settle this issue. Chu *et al.* reported artificial control over ferroelectric domain structures through the use of various vicinal $SrTiO_3$ (STO) substrates.[8] Recently, a nearly tetragonal BFO phase (space group *P*4*mm*) with a large c/a ratio (∼1.27) was predicted and demonstrated to have a giant spontaneous polarization (∼150 μC/cm^2).[10–13] The stress-induced structural phase transition from rhombohedral-like phase to tetragonal-like phase and high piezoelectric response make BFO even more promising. Although there are abundant studies on BFO films, there are still some controversies about its phase transition. Strong deviations from the properties of thicker films were often observed. Thus, reducing thickness appears as another way to tailor film properties and bring exciting novel functionalities to electronics and spintronics.[14] Very thin multiferroic films have been investigated for a couple of years. However, very thin (< 30 nm) BFO films have rarely been reported.[15,16] Furthermore, BFO thin films are commonly grown on STO (001) surfaces,[3,7,15] while the BFO film on polar STO (111) surface has seldom been studied. The progress in thin-film deposition techniques enables the control of thin-film growth at the unit-cell level. In this work, we report the structural properties of very thin BFO films epitaxially grown on STO (001) and polar (111) surfaces.

2. Experimental details

BFO thin films were directly grown on TiO_2-terminated STO (001) and Ti-terminated STO (111) substrates by oxygen plasma-assisted molecular beam epitaxy (OPAMBE) in a custom designed MBE/XPS system (SPECS GmbH). Commercial STO (001) and STO (111) single crystals were used. The STO substrates were etched in NH_4F-buffered HF (BHF) solution (pH = 4.5) for 2 min, and rinsed with deionized water and then dried in nitrogen stream. Prior to the growth of BFO films, STO substrates were thermally annealed at 800 °C for 20 min under radical oxygen flux. Bi and Fe were co-evaporated by K-cells using high-purity solid sources. Because of very low sticking coefficient of Bi, the atomic flux ratio of Bi:Fe was set at 7:1 measured by an *in situ* quartz

*Project supported by the National Basic Research Program of China (Grant Nos. 2009CB929202 and 2013CB922303), the National Natural Science Foundation of China (Grant Nos. 51231007 and 11374189), the Funding from Shandong University, China (Grant No. 2011JC006), and the Electronics Technology Group Corporation of China (Grant No. CJ20130304).

†Corresponding author. E-mail: liu-guolei@sdu.edu.cn

© 2014 Chinese Physical Society and IOP Publishing Ltd

microbalance. A radio-frequency oxygen plasma source (Oxford Scientific) was used to provide reactive oxygen radicals. The oxygen partial pressure during growth was 5×10^{-4} Pa. The BFO thin film was grown at very low growth speed of 0.1 nm/min at 440 °C. The growth process was monitored by real-time reflection high-energy electron diffraction (RHEED). The crystal structure of BFO thin films were characterized by a high-resolution X-ray diffractometer (HRXRD). The chemical composition and oxidation states of Fe were determined by *in situ* X-ray photoelectron spectroscopy (XPS). The morphology and domain structures of BFO films were characterized by atomic force microscopy (AFM) and piezoelectric force microscopy (PFM), respectively. The absorption spectra were measured using UV–visible spectrometer. For electric and dielectric measurements, conductive Nb-doped STO substrates were used as bottom electrodes. Top Pt electrodes with diameters of 50–500 μm were fabricated by e-beam evaporation through lift-off technique. Leakage currents were characterized using an Agilent B1500A semiconductor characterization system.

3. Results and discussion

Figures 1(a) and 1(b) show the RHEED patterns for BFO thin films grown on STO (001) and STO (111) surfaces, respectively. The stripped RHEED pattern indicates layer-by-layer growth mode of BFO film on STO (001) surface, while elongated dotted RHEED pattern indicates three-dimensional (3D) growth mode on STO (111) surface. Figures 1(c) and 1(d) show AFM images of a 15-nm BFO film grown on STO (001) and a 20-nm BFO film on STO (111). The root-mean-square (RMS) roughness for Figs. 1(c) and 1(d) are 0.27 nm and 9.31 nm. The rougher morphology of BFO/STO (111) can be attributed to 3D growth mode, which is caused by the high bond density of the pseudo cubic (111) face.[16,17]

XRD measurements were used to examine the structural properties of epitaxial BFO films. Figure 2(a) shows θ–2θ XRD scan of a BFO(15 nm)/STO (001) heterostructure. The scan shows that BFO is aligned with its [001] axis normal to STO (001) surface, and no other reflection peak is found. The full width at half maximum (FWHM) of (002) peak of BFO is 0.35° (see the ω rocking curve in Fig. 2(c)). The ϕ scans of (011) reflection of both BFO film and STO substrate have four-fold symmetry, as shown in Fig. 2(e). The one-peak shape of ϕ scan indicates that (001)-oriented BFO film is one variant and no twin structure is observed.[18] The XRD θ–2θ and ϕ scans indicate that the epitaxial relation is (001)[100]BFO‖(001)[100]STO. The four-fold symmetry and one-variant structure indicate that the BFO film grown on STO (001) is a fully strained tetragonal phase, which is different from the rhombohedral phase in either BFO thick films[19] or bulk BFO crystals. BFO film grown on STO (111) has different crystal structures. Figure 2(b) shows the XRD θ–2θ scan of a BFO(20 nm)/STO (111) heterostructure, where the BFO is aligned with its $[0001]_h$ (where subscript h denotes hexagonal indices) axis normal to the STO (111) surface and no other reflection peak is found. Figure 2(f) shows the ϕ scans of BFO $(2\bar{1}\bar{1}3)_h$ and $(10\bar{1}2)_h$ diffraction peaks. The six-fold symmetry of $(2\bar{1}\bar{1}3)_h$ family shows that $(0001)_h$-oriented BFO film is a low-symmetry rhombohedral ($R3c$ symmetry) phase.[16] The three peaks of $(10\bar{1}2)_h$ family indicate a single in-plane orientation and untwinned BFO film.[16] The XRD θ–2θ and ϕ scans indicate that the epitaxial relationship of BFO/STO (111) is $(0001)_h[2\bar{1}\bar{1}0]_h$BFO‖(111)$[1\bar{1}0]$STO. The ω rocking curve in Fig. 2(d) shows that the FWHM of BFO $(0006)_h$ peak is 0.3°.

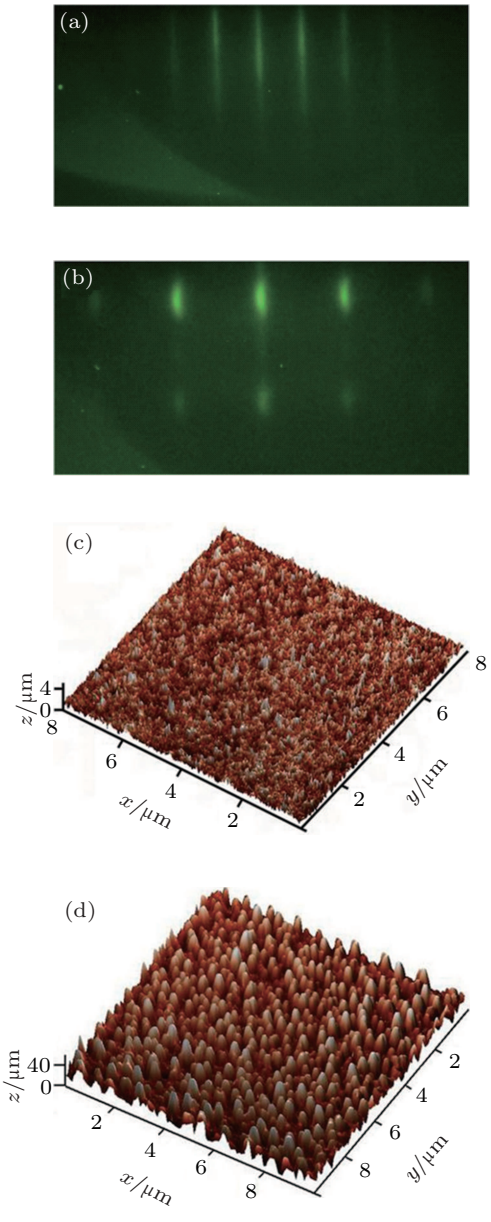


Fig. 1. (color online) RHEED patterns of BFO films grown on (a) STO (001) and (b) STO (111). AFM images of BFO films grown on (c) STO (001) and (d) STO (111).

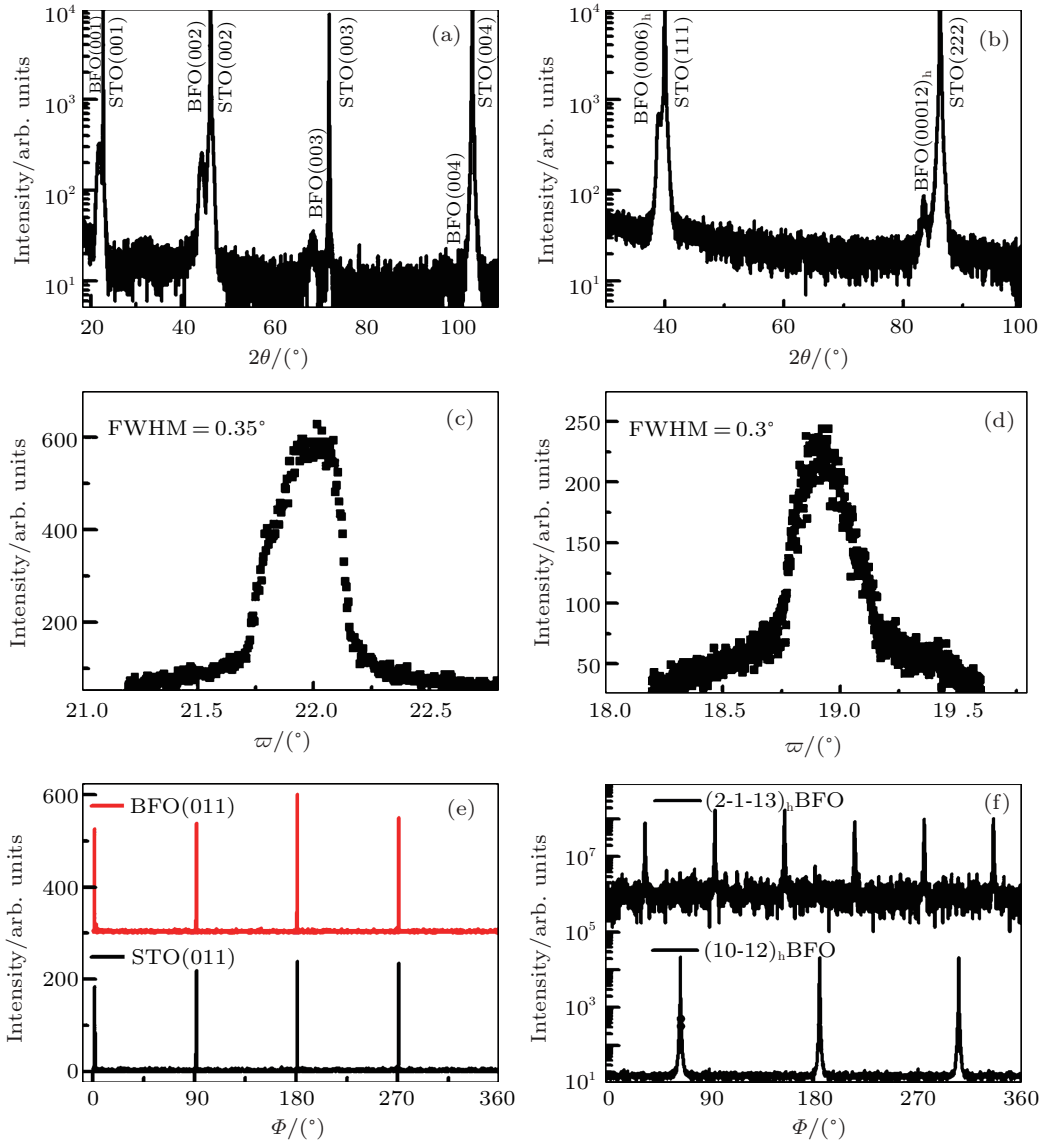


Fig. 2. (color online) θ–2θ X-ray diffraction patterns of (a) a 15-nm BFO film grown on STO (001) and (b) a 20-nm BFO film on STO (111). Rocking curves of (c) BFO (002) peak for BFO/STO (001) and (d) BFO $(0006)_h$ peak for BFO/STO(111). (e) ϕ scans of BFO (011) and STO (011) reflection for BFO/STO (001). (f) ϕ scan of BFO and reflections for BFO/STO (111).

The Fe 2p core-level spectra of BFO/STO (001) and BFO/STO (111) heterostructures were characterized by *in situ* XPS measurements. Figure 3 shows a typical XPS spectrum of as-grown BFO(15 nm)/STO (001) at binding energy around Fe 2p. The Fe 2p is split into $2p_{3/2}$ and $2p_{1/2}$ doublets due to spin–orbit coupling, which are located at 711 eV and 724.6 eV, respectively. A peak located at 719 eV is observed, which corresponds to the shake-up satellite peak of Fe^{3+}.[20] The shake-up satellite peak of Fe^{2+}, which is located at 716 eV,[20] is absent in our BFO film. The BFO/STO (111) shows similar XPS spectrum (not shown here). The XPS measurements indicate that the chemical state of iron in our BFO films is Fe^{3+},[21] and excludes of Fe^{2+} states which may refer to possible phases of FeO, Fe_3O_4, etc.

The band gap and defect states of epitaxial BFO films are important for device applications. The direct method to characterize them is the absorption spectrum. Figure 4(a) shows the UV–visible absorption spectra of BFO(12 nm)/STO (001) and BFO(20 nm)/STO (111) at room temperature. The rapid rise in absorbance around 2.65 eV is attributed to the

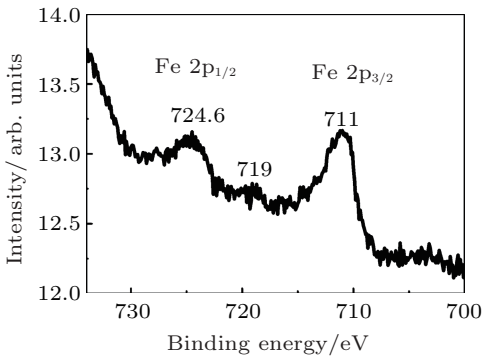


Fig. 3. X-ray photoemission spectrum of Fe 2p in an as-grown 15-nm BFO film on STO (001).

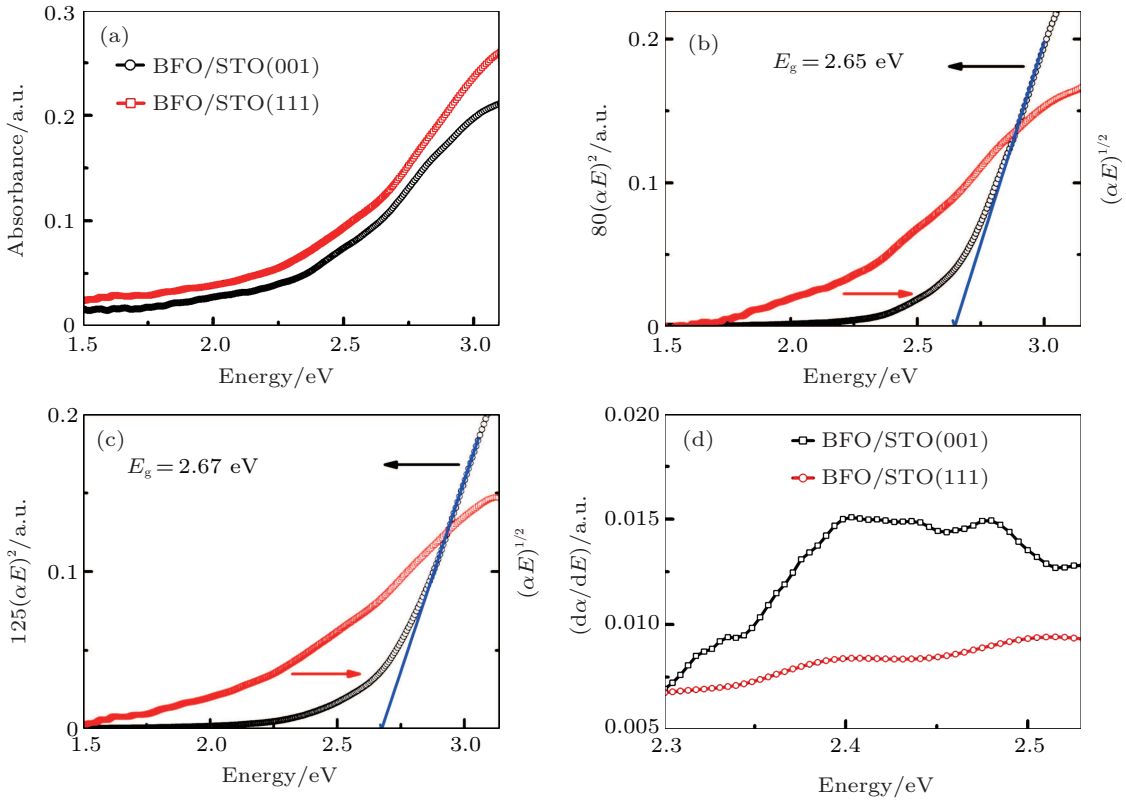


Fig. 4. (color online) UV–visible absorption spectra of BFO films. (a) Optical absorption of a 12-nm thick BFO film grown on STO (001) and a 20-nm BFO film on STO (111) substrate. Plots of $(\alpha E)^2$ and $(\alpha E)^{1/2}$ versus photon energy E for (b) BFO/STO (001) and (c) BFO/STO (111), respectively. A linear extrapolation of $(\alpha E)^2$ to 0 suggests a direct band gap at 2.65 eV and 2.67 eV. (d) Plots of $d\alpha/dE$ versus photon energy E for BFO/STO (001) and BFO/STO (111).

fundamental absorption of BFO films. To determine the band gap, the absorption coefficient $\alpha(E)$ is fitted by considering the direct and indirect absorption transitions[22]

$$a(E) = \frac{A}{E}(E - E_{g,d})^{1/2} + \frac{B(E - E_{g,i} \pm E_p)^2}{E\left[\exp\left(\frac{E_p}{kT} - 1\right)\right]}, \quad (1)$$

where A and B are constants, E_p is the energy of emitted or absorbed phonon, and $E_{g,d}$ and $E_{g,i}$ are the magnitudes of direct and indirect band gaps, respectively. This model allows for the extraction of $E_{g,d}$ and $E_{g,i}$ by plotting $(\alpha E)^2$ and $(\alpha E)^{1/2}$ as functions of photon energy, separately. Figure 4(b) plots $(\alpha E)^2$ and $(\alpha E)^{1/2}$ as functions of photon energy E for BFO/STO (001), and figure 4(c) plots $(\alpha E)^{1/2}$ and $(\alpha E)^{1/2}$ as functions of photon energy E for BFO/STO (111). The good fitting of $(\alpha E)^2$ indicates that the BFO on both STO (001) and STO (111) are direct band gap.[23] The direct band gaps can be determined by the linear extrapolation $(\alpha E)^2$ to 0, which are 2.65 ± 0.05 eV and 2.67 ± 0.05 eV for BFO/STO (001) and BFO/STO (111), respectively. These values are consistent with recent theoretical[24] and experimental results.[15,25] Figure 4(d) displays the plots of $d\alpha/dE$ versus E in the range of 2.3–2.53 eV. The peaks reveal that there are sub-band gap defect states which are possibly caused by oxygen vacancies and/or Bi vacancies. Similar defect states were reported for BFO thin films grown on $DyScO_3$, Nb-STO,[26] and STO substrates.[27] It is noted that BFO grown on STO (111) surface has less defect states than BFO on STO (001) surface.

Figure 5(a) shows the dielectric constant and dielectric loss as functions of frequency for BFO films grown on conductive Nb-doped STO (001) and STO (111) substrates. Compared to BFO/STO (001), BFO/STO (111) has weaker frequency-dependent dielectric constant and lower dielectric loss due to less space charge which is induced by defects in BFO film, such as oxygen vacancies and/or Bi vacancies.[28] Figure 5(b) shows leakage current density J–E curves of Pt/BFO(20 nm)/Nb-STO (001) and Pt/BFO(24 nm)/Nb-STO (111) capacitors. The J–E curves are asymmetric at negative and positive voltage biases, which are attributed to different work functions of bottom Nb-doped STO and top Pt electrodes.[17] At an electric field of -100 kV/cm, the leakage current density is 3.4×10^{-5} A/cm^2 for Pt/BFO/Nb-STO (001) and 4.5×10^{-6} A/cm^2 for Pt/BFO/Nb-STO (111), respectively, which are much lower than the leakage current density reported by other groups.[7,29] Figures 5(c) and 5(d) show the in-plane PFM images of BFO films. BFO/STO (001) has irregular partial domain structure, while BFO/STO (111) shows unique homogeneous domain structure. Out-of-plane PFM images of both BFO films show uniform contrast (not shown), indicating that BFO/STO (111) exhibits a single-domain behavior.

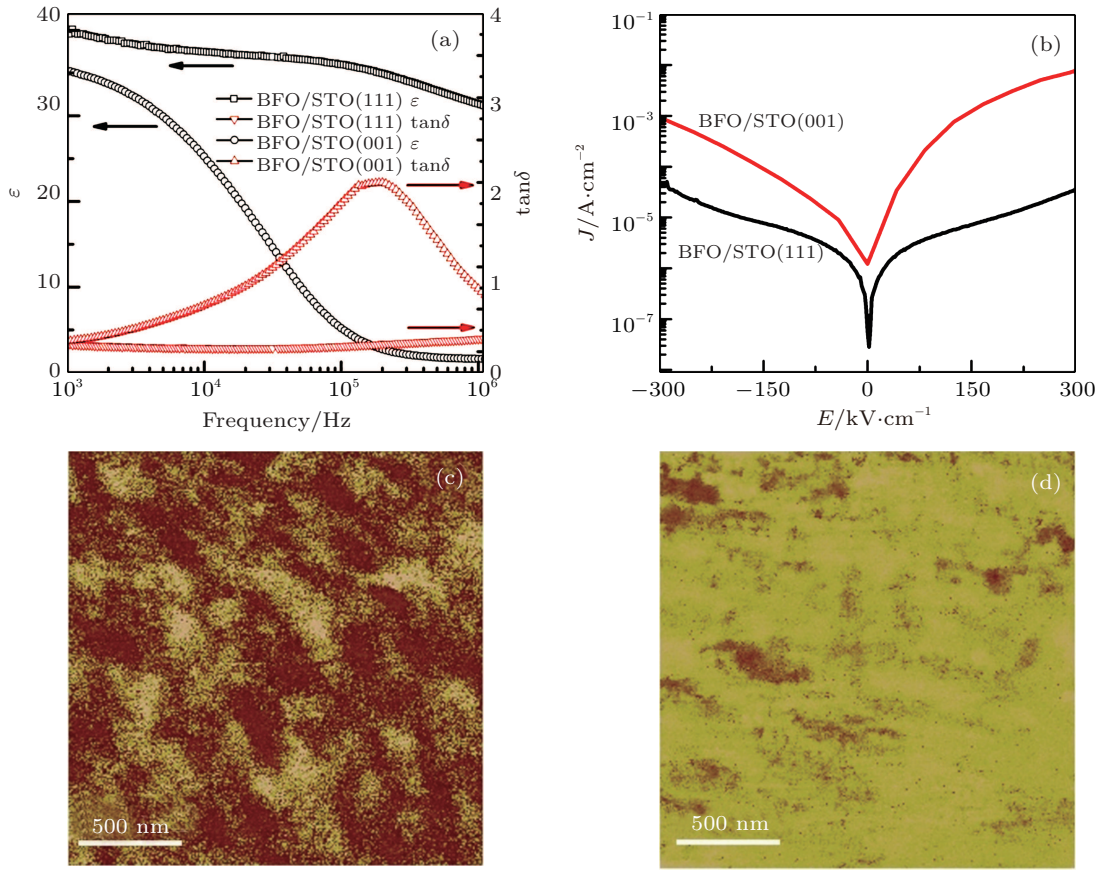


Fig. 5. (color online) (a) Dielectric constant and dielectric loss for BFO/Nb-STO (001) and BFO/Nb-STO (111). (b) *J*–*E* characteristics of Pt/BFO(20 nm)/Nb-STO (001) and Pt/BFO(24 nm)/Nb-STO (111) capacitors. In-plane PFM images of BFO films grown on (c) Nb-STO (001) and (d) Nb-STO (111).

As mentioned previously, the very thin BFO films were grown epitaxially on STO substrates. BFO/STO (001) is a fully strained tetragonal phase with epitaxial relationship (001)[100]BFO‖(001)[100]STO, and BFO/STO (111) is a fully strained rhombohedral phase with orientation relationship $(0001)_h$BFO‖(111)STO. Therefore, the BFO films grown on STO (001) and STO (111) surfaces have the same lattice mismatch. The discrepancy on surface morphology, dielectric and ferroelectric properties are not due to the lattice mismatch, which are possibly induced by the polarity of BFO films and underneath STO surfaces. Since the tetragonal BFO epilayer and STO (001) surface are nonpolar, the polarity has less influence on the BFO epilayer which results in a two-dimensional (2D) growth mode with smooth surface morphology at very thin film region. On the contrary, both of STO (111) and above BFO epilayer have the electric polarization in the [111] axis. Depending on the relative polarity of STO (111) and above BFO epilayer, the parallel and anti-parallel polarization geometries reveal different surface energy, which causes the rougher surface morphology. It is also noticed that the tetragonal BFO epilayer has four equivalent rhombohedral distortions along the {111} directions, which induces more defect states than BFO/STO (111) film, as shown by the optical absorption measurements in Fig. 4. The defect states will introduce more space charges which reduce the dielectric constants and increase the dielectric loss at high frequency (see Fig. 5(a)). Additionally, the space charge will also increase the leakage current density on BFO/STO (001) (see Fig. 5(b)). Since the rhombohedral distortion of BFO/STO (111) is perpendicular to STO(111) surface, there is no component in plane, which shows a unique homogeneous domain structure in Fig. 5(d), while BFO/STO (001) indicates in-plane domain structures, as shown in Fig. 5(c).

4. Conclusions

In summary, phase-pure, untwined, very thin BFO films are epitaxially grown by OPAMBE. BFO/STO (001) is a fully strained tetragonal phase with epitaxial relationship (001)[100]BFO‖(001)[100]STO. BFO/STO (111) is a rhombohedral phase with orientation relationship $(0001)_h[2\bar{1}\bar{1}0]_h$BFO‖(111)[1$\bar{1}$0]STO. *In situ* XPS confirms Fe^{3+} in these BFO films. The direct band gaps are 2.65 eV and 2.67 eV for BFO films on STO (001) and STO (111), respectively. BFO/STO (111) has less defect states than BFO/STO (001), which results in reduced leakage and lower dielectric loss. PFM measurement reveals that BFO/STO (001) has an irregular domain structure, while BFO/STO (111) exhibits a single domain behavior.

References

[1] Spaldin N A and Fiebig M 2005 *Science* **309** 391

[2] Eerenstein W, Mathur N D and Scott J F 2006 *Nature* **442** 759

[3] Zhao T, Scholl A, Zavaliche F, Lee K, Barry M, Doran A, Cruz M P, Chu Y H, Ederer C, Spaldin N A, Das R R, Kim D M, Baek S H, Eom C B and Ramesh R 2006 *Nat. Mater.* **5** 823

[4] Ramesh R and Spaldin N A 2007 *Nat. Mater.* **6** 21

[5] Kubel F and Schmid H 1990 *Acta Crystallogr. B* **46** 698

[6] Streiffer S K, Parker C B, Romanov A E, Lefevre M J, Zhao L, Speck J S, Pompe W, Foster C M and Bai F R 1998 *J. Appl. Phys.* **83** 2742

[7] Jang H W, Ortiz F, Baek S H, Folkman C M, Das R R, Shafer P, Chen Y, Nelson C T, Pan X, Ramesh R and Eom C B 2009 *Adv. Mater.* **21** 817

[8] Chu Y H, Cruz M P, Yang C H, Martin L W, Yang P L, Zhang J W, Lee K, Yu P, Chen L Q and Ramesh R 2007 *Adv. Mater.* **19** 2662

[9] Shelke V, Mazumdar D, Srinivasan G, Kumar A, Jesse S, Kalinin S, Baddorf A and Gupta A 2011 *Adv. Mater.* **23** 669

[10] Hatt A J, Spaldin N A and Ederer C 2010 *Phys. Rev. B* **81** 054109

[11] Ederer C and Spaldin N A 2005 *Phys. Rev. Lett.* **95** 257601

[12] Zeches R J, Rossell M D, Zhang J X, Hatt A J, He Q, Yang C H, Kumar A, Wang C H, Melville A, Adamo C, Sheng G, Chu Y H, Ihlefeld J F, Erni R, Ederer C, Gopalan V, Chen L Q, Schlom D G, Spaldin N A, Martin L W and Ramesh R 2009 *Science* **326** 977

[13] Zhang J W, He Q, Trassin M, Luo W, Yi D, Rossell M D, Yu P, You L, Wang C H, Kuo C Y, Heron J T, Hu Z, Zeches R J, Lin H J, Tanaka A, Chen C T, Tjeng L H, Chu Y H and Ramesh R 2011 *Phys. Rev. Lett.* **107** 147602

[14] Gajek M, Bibes M, Fusil S, Bouzehouane K, Fontcuberta J, Barthélémy A and Fert A 2007 *Nat. Mater.* **6** 296

[15] Ihlefeld J F, Podraza N J, Liu Z K, Rai R C, Xu X, Heeg T, Chen Y B, Li J, Collins R W, Musfeldt J L, Pan X Q, Schubert J, Ramesh R and Schlom D G 2008 *Appl. Phys. Lett.* **92** 142908

[16] Ihlefeld J F, Kumar A, Gopalan V, Schlom D G, Chen Y B, Pan X Q, Heeg T, Schubert J, Ke X, Schiffer P, Orenstein J, Martin L W, Chu Y H and Ramesh R 2007 *Appl. Phys. Lett.* **91** 071922

[17] Tian W, Vaithyanathan V, Schlom D G, Zhan Q, Yang S Y, Chu Y H and Ramesh R 2007 *Appl. Phys. Lett.* **90** 172908

[18] Béa H, Bibes M, Petit S, Kreisel J and Barthélémy A 2007 *Phil. Mag. Lett.* **87** 165

[19] Qi X, Wei M, Lin Y, Jia Q, Zhi S, Dho J, Blamire M G and Manus-Driscoll J L 2005 *Appl. Phys. Lett.* **86** 071913

[20] Schedel-Niedrig T, Weiss W and Schlögl R 1995 *Phys. Rev. B* **52** 17449

[21] Singh S K, Ishiwara H and Maruyama K 2006 *J. Appl. Phys.* **100** 064102

[22] Pankove J I *Optical Processes in Semiconductors* (Englewood: Prentice-Hall) p. 1971

[23] Béa H, Dupé B, Fusil S, Mattana R, Jacquet E, Warot-Fonrose B, Wilhelm F, Rogalev A, Petit S, Cros V, Anane A, Petroff F, Bouzehouane K, Geneste F, Dkhil B, Lisenkov S, Ponomareva I, Bellaiche L, Bibes M and Barthélémy A 2009 *Phys. Rev. Lett.* **102** 217603

[24] Clark S J and Robertson J 2007 *Appl. Phys. Lett.* **90** 132903

[25] Kumar A, Rai R C, Podraza N J, Denev S, Ramirez M, Chu Y, Martin L W, Ihlefeld J, Heeg T, Schubert J, Schlom D G, Orenstein J, Ramesh R, Collins R W, Musfeldt J L and Gopalan V 2008 *Appl. Phys. Lett.* **92** 121915

[26] Himcinschi C, Vrejoiu I, Friedrich M, Nikulina E, Ding L, Cobet C, Esser N, Alexe M, Rafaja D and Zahn D R T 2010 *J. Appl. Phys.* **107** 123524

[27] Hauser A J, Zhang J, Mier L, Ricciardo R A, Woodward P M, Gustafson T L, Brillson L J and Yang F Y 2008 *Appl. Phys. Lett.* **92** 222901

[28] Cui Y F, Zhao Y G, Luo L B, Yang J J, Chang H, Zhu M H, Xie D and Ren T L 2010 *Appl. Phys. Lett.* **97** 222904

[29] Yang H, Jain M, Suvorova N A, Zhou H, Luo H M, Feldmann D M, Dowden P C, DePanla R F, Foltyn S R and Jia Q X 2007 *Appl. Phys. Lett.* **91** 072911